Euler–Euler Numerical Model for Transport Phenomena Modeling in a Natural Circulation Loop Operated by Nanofluids

Blaž Kamenik[1] · Nejc Vovk[1] · Elif Begum Elcioglu[2] · Firat Sezgin[2] · Erdem Ozyurt[2] · Ziya Haktan Karadeniz[3] · Alpaslan Turgut[4] · Jure Ravnik[1]

Abstract

This paper explores a computational approach to model multiphase heat transfer and fluid flow in a natural circulation loop utilizing nanofluids. We propose and implement an Euler–Euler framework in a CFD environment, incorporating an innovative boundary condition to preserve mass conservation during thermophoretic particle flux. The model's accuracy is verified through a one-dimensional example, by comparing results against both an Euler–Lagrange model and an in-house finite volume solution. Experimental validation is conducted with aluminum oxide nanofluids at varying nanoparticle concentrations. We prepared the nanofluids and measured their thermophysical properties up to 60°C. We assess the thermal performance of the nanofluid in natural circulation loop at different heating powers via experiment and numerical simulations. The findings reveal that the heat transfer enhancement offered by the nanofluid is modest, with minimal differences observed between the proposed Euler–Euler approach and a simpler single-phase model. The results underscore that while the Euler–Euler model offers detailed particle–fluid interactions, its practical thermal advantage is limited in this context.

List of symbols

Γ	Ansys Fluent implementation of the diffusion term
λ	Thermal conductivity [W·(m^{-1}·K^{-1})]
μ	Dynamic viscosity [Pa·s]
$\frac{\partial}{\partial n}$	Normal derivative, $\nabla \cdot \vec{n}$
ϕ	Scalar field
ρ	Density [kg·m^{-3}]
τ	Stress tensor [Pa]
φ	Nanoparticle volume fraction [-]

Extended author information available on the last page of the article

 Springer

$\vec{F}$ Ansys Fluent implementation of the advection term
$\vec{j}_p$ Nanoparticle mass flux [kg·(m^{-2} ·s^{-1})]
$\vec{u}$ Velocity field [m/s]
A Area [m^2]
c_p Specific heat capacity [J·(kg^{-1}K^{-1})]
D_B Brownian diffusion coefficient [m^2·s^{-1}]
d_p Nanoparticle diameter [m]
D_T Thermophoretic diffusion coefficient [m^2·s^{-1}]
G Temperature gradient [K·m^{-1}]
g Gravitational acceleration [m·s^{-2}]
k_B Boltzmann constant [J·K^{-1}]
L Characteristic length [m]
p Pressure [Pa]
q Heat flux [W·m^{-2}]
R_i, M_i Fitting constants [-]
S Ansys Fluent implementation of the source term
Sh Heat source term [W · m^{-3}]
T Temperature [K]
t Time [s]
x, y, z Cartesian coordinates

1 Introduction

It has been more than twenty years since Choi and Eastman [1] introduced the concept of dispersion of nanoparticles in base fluids, the so-called nanofluids, and emphasized their potential due to their high thermal conductivity. Since then, extensive experimental and numerical research [2–9] has expanded our understanding of the benefits of nanofluids in a wider range of systems and applications. At the same time, the challenges nanofluids present have also been increasingly recognized.

On the one hand, study of nanofluids is an active research topic in chemical science [10–14], where subjects such as stability, synthesis methods, and thermophysical properties are of interest. On the thermal engineering side, one of the challenges is the performance of numerical simulations. Numerical simulations are routinely used in the development of heat exchangers [15] and other heat transfer devices where a nanofluid is a possible working fluid. The uncertainty in predicting the heat transfer performance of devices working with nanofluids is still large in numerical simulations [16]. Recently, a numerical round-robin study, in which several research groups looked at the same very simple heat exchanger operating with a nanofluid [17] showed that the simulation results differ greatly when using different approaches, such as different mathematical models of the nanofluid or the use of different numerical methods. Similar conclusions were drawn in other studies comparing different mathematical models to describe the transport phenomena with

nanofluids [18]. As will all active research fields, the use of artificial intelligence (A.I.) supported techniques is also popular [19, 20].

In this work, we aim to contribute to the pool of knowledge on numerical modeling of transport phenomena using nanofluids in a nanofluid-based natural circulation loop. We present two approaches for modeling nanofluids and compare them with experimental measurements. The approaches compared in this work are the single-phase approach and the Euler–Euler approach. We model nanofluids with the single-phase approach only for the sake of comparison. The novelty of this research lies in our implementation of the Euler–Euler approach. The starting point is the mathematical description proposed by Buongiorno [21–25]. We then propose a novel implementation of the model in the commercial CFD code Ansys Fluent and introduce a mass-preserving boundary condition that has to be specifically developed to treat both the diffusive and thermophoretic particle mass fluxes.

The developed method is verified with experimental measurements of temperatures in a natural circulation loop (NCL). NCLs are passive systems without moving or rotating mechanical parts. The density gradient between the hot and cold sides drives the system so that it can transfer heat from one side to the other by natural convection. We have developed a single-phase system in which the density gradient is caused solely by a temperature gradient and there is no phase change. This type of system has a wide range of applications due to its simplicity and reliability [26]. They are used in various technical applications, including cooling turbine blades, solar water heaters [27], core of nuclear reactors, cooling electronic chips, and for refrigeration.

The main objective of this paper is to present and evaluate a numerical Euler–Euler modeling framework for the simulation of multiphase heat transfer and fluid flow in a nanofluid-driven NCL. The main objectives are as follows: to develop and implement the Euler–Euler model using a novel mass-conserving boundary condition to treat the thermophoretic particle flux. The model is then experimentally validated and used to evaluate the heat transfer enhancement of NCL operated with nanofluids. Finally, we compare the new model with a simpler single-phase approach.

2 Materials and Methods

The aim of this study is to simulate the flow of a nanofluid using two different modeling approaches: the Euler–Euler approach and the single-phase approach. The nanofluid consists of a base fluid with dispersed nanoparticles that improve its thermal properties.

In the Euler–Euler modeling approach, the flow of the nanofluid is modelled using the Buongiorno [21] mixture model. This model treats the base fluid and the nanoparticles as two interacting continua and captures the relative motion between them. Various physical mechanisms, including Brownian diffusion and thermophoresis, influence the interaction between the nanoparticles and the fluid. A major challenge arises at the boundaries where either the heat flux or the temperature is fixed. The presence of thermophoresis leads to an inconsistency in mass conservation when the

standard "no-flux" boundary condition is used for the concentration of nanoparticles in a closed system. To solve this problem and ensure the correct conservation of nanoparticle mass, the thermophoretic term was added to the advective term.

The single-phase approach, on the other hand, treats the nanofluid as a homogeneous fluid with measured thermophysical properties, such as thermal conductivity and viscosity, based on the volume concentration of the nanoparticles. The key assumption in this approach is that the concentration of nanoparticles remains uniform throughout the entire region, which means that the relative movement between the nanoparticles and the base fluid is neglected. This simplifies the flow to a single-phase scenario, which is computationally less demanding, but does not provide the ability to capture the detailed interactions present in the Euler–Euler approach, which provides a more complete picture that is resembling the actual nanofluid flow

One of the biggest challenges with the Euler–Euler approach was to ensure mass conservation at the boundaries due to thermophoretic effects. In contrast, the single-phase model assumes a uniform concentration of nanoparticles, which simplifies the modeling, but at the cost of potentially overlooking complex interactions present between fluid and particles.

2.1 Experiments

2.1.1 Measurement of Nanofluid Thermophysical Properties

For the experiments presented in this work, we prepared Al_2O_3-water nanofluids with 0.5, 1, and 2 vol. % by the two-step method. 25 nm-sized Al_2O_3 nanoparticles of necessary amounts (measured via WSA-224 analytical balance) to prepare the target concentrations were mixed with deionized water using magnetic stirring for 30 min (using a MTOPS HSD180 magnetic stirrer) at 500 rpm. No stabilizing additives were added and the samples were not further homogenized or ultrasonicated. The thermophysical characterization of the samples includes measurements of viscosity and thermal conductivity, which were performed for different concentrations of nanoparticles and sample temperatures.

The viscosity measurements were carried out using the SV-10 sine-wave vibro viscometer, which works according to the tuning fork vibration method [28]. The viscometer has a measuring range of $0.3 - 10^4$ $mPas$. During the measurements, the temperature of the sample was modulated between $20 - 60\,°C$ in a container equipped with a water jacket using a Mikrotest water circulation bath. The viscometer was calibrated using water as a reference fluid and a one-point calibration with water was performed between each nanofluid measurement.

The thermal conductivity of the samples was measured with the modulated hot-wire sensor (HW), which is based on a hot-wire thermal probe with alternating current excitation and 3ω lock-in detection [29]. In the 3ωHW method, the hot wire on the probe is immersed in the fluid sample. It acts both as a heating element to excite the fluid and as a sensing element to measure the temperature rising around the wire, which depends on the thermal conductivity of the sample. The wire is excited by a sinusoidal voltage with a fundamental frequency of "ω." The excitation causes

a power dissipation in the wire with the frequency "2ω" and it causes a temperature oscillation at the interface between the wire and the fluid with the same frequency "2ω." Since the temperature oscillation causes a simultaneous oscillation of the resistance of the HW with 2ω, the excitation current generates the 3rd harmonic magnitude (3ω voltage) at the HW probe. The method was validated with pure fluids such as water, methanol, ethanol, and ethylene glycol and provided accurate thermal conductivity ratios within $\pm 2\%$. Further details about the setup can be found elsewhere [30, 31].

2.1.2 Experiments With the Natural Circulation Mini Loop

To validate the proposed numerical approach, we performed an experiment with an aluminum oxide nanofluid in a natural circulation loop. The loop was built from copper pipes, as they have good thermal properties and good moldability (see Fig. 1a). Plastic pipes were used as an extension of the inlet section designed to create a fluid inlet that also served as an expansion vessel and became an easily accessible fluid change point for the user. It was decided to measure the temperature of the fluid. As the measuring diameter of the thermocouples used is 1 *mm*, inserting the thermocouple into the pipe creates a 5% blockage in the flow area. To limit the effect of this blockage on the flow, the thermocouples were placed in contact with the flow and close to the inner wall. A sufficient length of nickel–chromium heating wire was wound around the heating area of the system to provide the required power input. Power input to the system is provided by controlling the current and voltage with the Aim-TTi CPX400DP programmable DC power supply. The uncertainties for the power input are calculated as 1.11%, 1.59%, and 3.9% for heating powers of 50 *W*, 30 *W*, and 10 *W*, respectively.

The installation of the brazed copper loop is shown in Fig. 1a. As the copper pipe is electrically conductive, an insulating tape with high thermal conductivity was applied around the heating area to prevent electrical contact between the heater and the copper pipe. The installation of the thermocouples used to measure the flow rate and their position on the pipe wall are shown in Fig. 2. After all thermocouples were installed, the system was tested for leaks. The system was operated for 2 h at different heating powers (10W, 30W, and 50W) with water
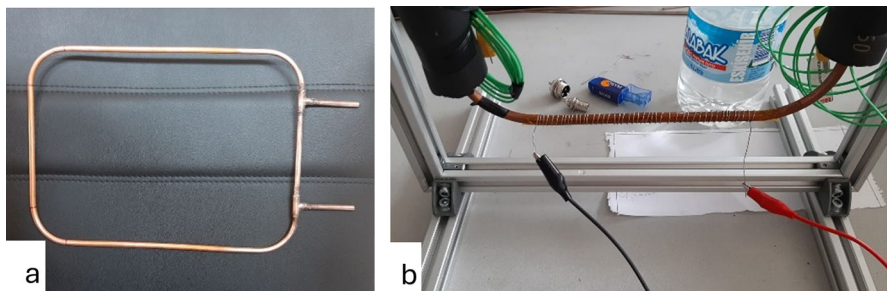

Fig. 1 (a) Copper loop after brazing. (b) Nickel-Chrome heater wire wrapped around the heater section
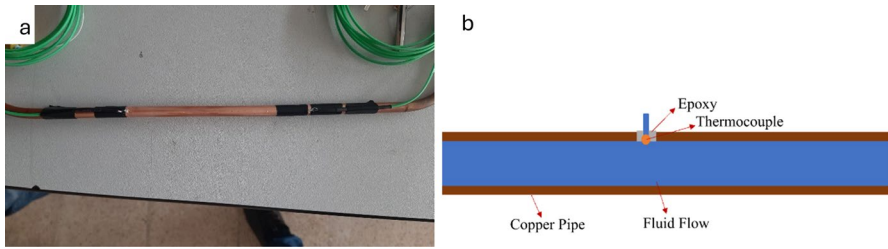
Fig. 2 (a) Loop section with thermocouples attached. (b) Axial location of the thermocouples on the copper pipe

added to the system. The system was then cooled down and switched on again. It was found that the system did not leak despite the expansion and contraction at varying heating powers. For the cooling area, a water jacket was made from ABS material using a 3D printer and then coated with epoxy resin to prevent leaks. The designed and manufactured water jacket can be seen in Fig. 3. After the water jacket was manufactured and coated with epoxy, the system was tested again for leaks. Following the leakage tests, the system was completely insulated. The experimental setup was then attached to a frame made of aluminum profiles
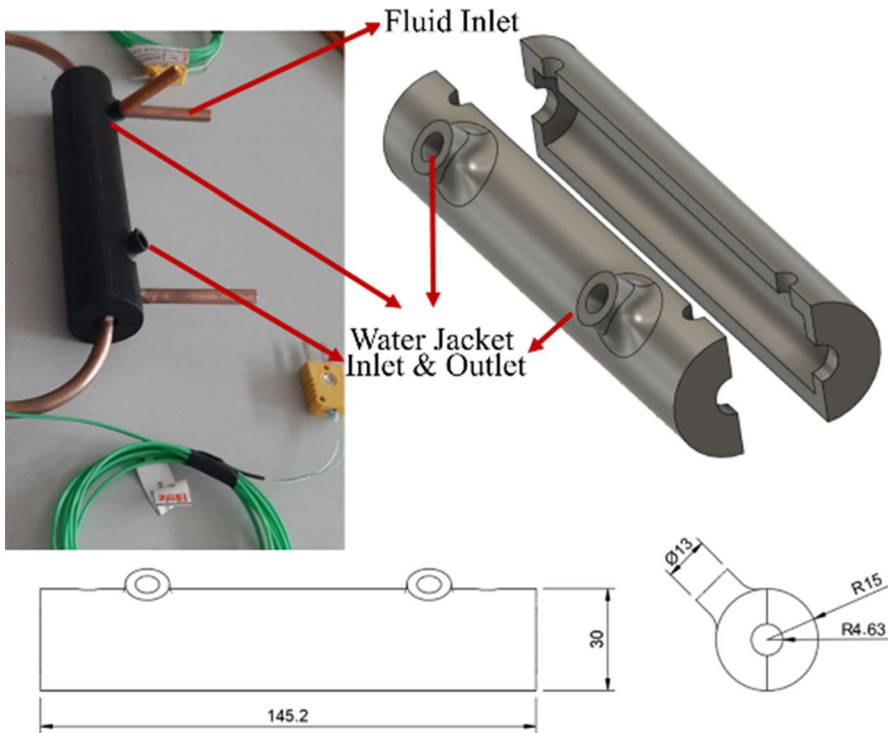
Fig. 3 Designed and produced water jacket for the cooling section

to hold the setup at a fixed angle. The system with all pipework ready for the experiments can be seen in Fig. 4b.

In the experimental setup, CLS CLRC-17 cooled circulation bath with 0.1^oC sensitivity was used to supply cooling water at a constant temperature. The power input to the system through the heater wire was ensured to be constant throughout the experiment with a voltage and current-controlled power supply. Experimental temperature data of the K-type thermocouples was logged via ORDEL UDL-100 Universal Data Logger. The uncertainty of a standard type-K thermocouple is generally defined as $\pm 0.75\%$ of the measured value or 0.5 °C below 100 °C [32]. Therefore, all the measurement errors are based on 0.5 °C of uncertainty for thermocouple readings. There are a total of eight thermocouples in the experimental setup, two for water jacket inlet and outlet, four for fluid temperature at both sides of the loop, and two for measuring heat loss in the heater area. See Fig. 5 for locations of T_{min} and T_{max} on the legs, which were used for comparisons. Temperature validation study on deionized water was performed for three different heater powers. The experiments were repeated twice with three days in between and the results were validated.

2.2 Numerical Model

The flow in a single-phase natural circulation loop, which we aim to model in this paper, is laminar and steady. The nanofluid is modeled as a Newtonian fluid with a temperature-dependent density. We model the nanofluid itself as well as the heat transfer in the pipe material. As the cooler is located above the heater, the hot fluid
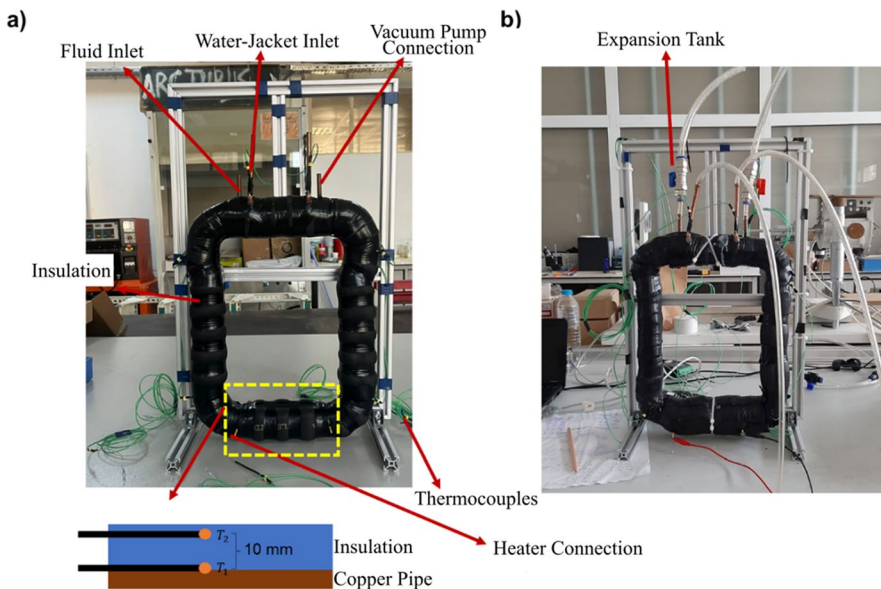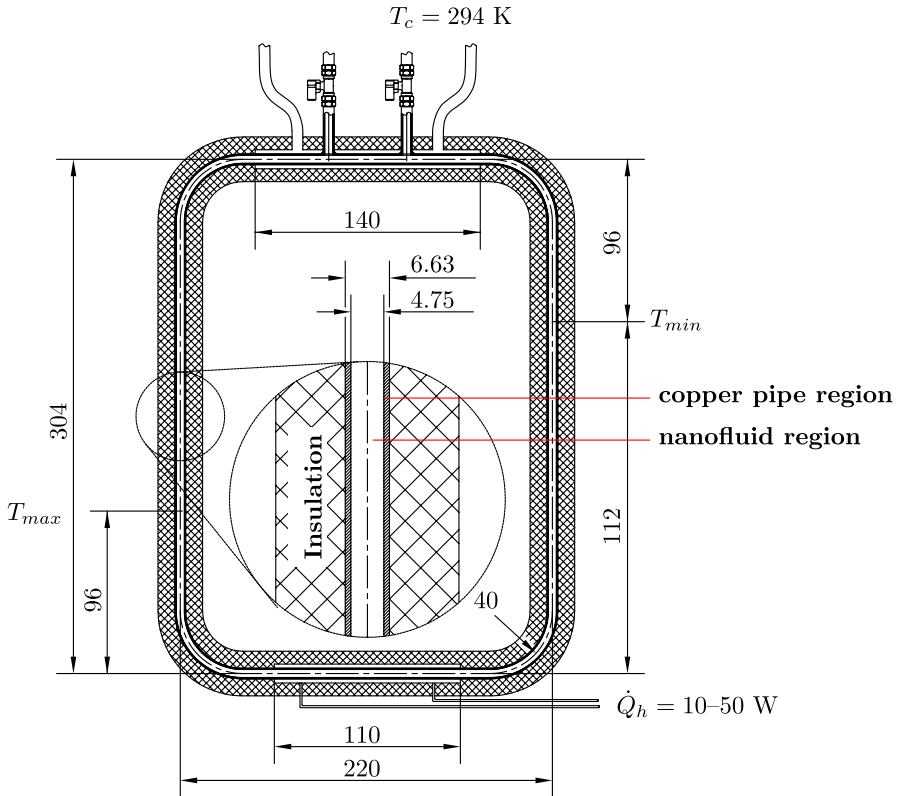

Fig. 4 Experiment setup

Fig. 5 Cross-section of the natural convection mini loop heat exchanger geometry. The cooling region is 140 mm long and the heating region is 110 mm long and the rest of the heat exchanger is insulated

flows upward and is cooled on the walls of the cooler. The cooled fluid then flows down the other side of the loop and is reheated when it reaches the heater. In this way, the natural circulation of the working fluid within the loop is established.

We propose the use of the Euler–Euler approach to model the flow of the nanofluid inside the loop. The continuity equation for the nanofluid is

$$\frac{\partial \rho_{nf}}{\partial t} + \nabla \cdot (\rho_{nf} \vec{u}) = 0 \tag{1}$$

where ρ_{nf} is the density of the nanofluid, t is the time, and $\vec{u}$ is the velocity field. The conservation of momentum is described by

$$\frac{\partial (\rho_{nf} \vec{u})}{\partial t} + \nabla \cdot (\rho_{nf} \vec{u}\vec{u}) = -\nabla p + \nabla \cdot \overline{\tau} + \rho_{nf} \vec{g}, \tag{2}$$

where p is the pressure, $\overline{\tau}$ is the stress associated with diffusive transport of momentum, and $\vec{g}$ is the gravitational acceleration. The energy equation is written in the following form:

$$\frac{\partial(\rho_{nf}c_{p,nf}T)}{\partial t} + \nabla \cdot (\vec{u}\rho_{nf}c_{p,nf}T) = \nabla \cdot (\lambda_{nf}\nabla T) + S_h \tag{3}$$

where $c_{p,nf}$ is the specific heat capacity of the nanofluid, T is the temperature, λ_{nf} is the thermal conductivity of the nanofluid and S_h is the heat source. In our case, we also solve one additional conservation equation for the nanoparticle volume concentration, φ.

In the Euler–Euler approach not only is the base fluid described with fields, also the nanoparticles are modeled via a concentration field. We use the volume fraction, φ, to describe nanoparticles behavior. The transport equation for the nanoparticle volume fraction in the absence of chemical reactions is as follows [21]:

$$\frac{\partial \varphi}{\partial t} + \vec{u} \cdot \nabla \varphi = -\frac{1}{\rho_p} \nabla \cdot \vec{j}_p, \tag{4}$$

where ρ_p is the nanoparticle density and $\vec{j}_p$ is the diffusion mass flux of the nanoparticles and represents the nanoparticle flux relative to the nanofluid velocity $\vec{u}$. If we assume that the external forces are negligible, $\vec{j}_p$ is the sum of only two diffusion terms: the Brownian diffusion and the thermophoresis:

$$\vec{j}_p = \vec{j}_{p,B} + \vec{j}_{p,T} = -\rho_p D_B \nabla \varphi - \rho_p D_T \frac{\nabla T}{T}. \tag{5}$$

Here, D_B is the Brownian diffusion coefficient, modeled by the Einstein–Stokes equation

$$D_B = \frac{k_B T}{3\pi \mu_w d_p}, \tag{6}$$

where k_B is the Boltzmann constant and d_p is the particle diameter. The viscosity μ_w is the viscosity of the base fluid–water. It is calculated as follows [33]:

$$\mu_w = 2.414 \cdot 10^{-5} \cdot 10^{\frac{247.8}{T-140.0}}, \tag{7}$$

where the temperature is given in Kelvin. The thermal diffusion coefficient D_T is calculated as

$$D_T = 0.26 \frac{\lambda_w}{(2\lambda_w + \lambda_p)} \frac{\mu_w}{\rho_w} \varphi, \tag{8}$$

where λ_p is the thermal conductivity of the nanoparticles and ρ_w is the density of water and is calculated as [33]

$$\rho_w = 821.27 + 1.4824 \cdot T - 0.002992 \cdot T^2, \tag{9}$$

where the temperature is given in Kelvin and λ_w is the thermal conductivity of water, which is calculated as follows [33]:

$$\lambda_w = 0.6065\left(-1.48445 + 4.12292\left(\frac{T}{298.15}\right) - 1.63866\left(\frac{T}{298.15}\right)^2\right) \quad (10)$$

with the temperature in Kelvin. The final form of the nanoparticle transport equation is as follows:

$$\frac{\partial \varphi}{\partial t} + \vec{u} \cdot \nabla \varphi = \nabla \cdot \left[D_B \nabla \varphi + D_T \frac{\nabla T}{T}\right]. \quad (11)$$

Equation 3 for the conservation of energy must be modified to take into account the additional heat flow caused by the movement of the nanoparticles. Therefore, we reformulate it by adding a source to the energy equation, S_h, which models the heat flow due to the motion of the nanoparticles:

$$S_h = \rho_p c_{p,p}\left(D_B \nabla \varphi + D_T \frac{\nabla T}{T}\right) \cdot \nabla T. \quad (12)$$

With this, we can rewrite the energy conservation equation for the mixture as follows:

$$\frac{\partial (\rho_{nf} c_{p,nf} T)}{\partial t} + \nabla \cdot (\vec{u} \rho_{nf} c_{p,nf} T) = \nabla \cdot \left(\lambda_{nf} \nabla T\right) + \rho_p c_{p,p}\left(D_B \nabla \varphi + D_T \frac{\nabla T}{T}\right) \cdot \nabla T. \quad (13)$$

The presented model is thus made up of four governing equations, describing the law of conservation of mass (Eq. 1), the law of conservation of momentum (Eq. 2), the law of conservation of energy (Eq. 13), and the law of conservation of volume for the nanoparticles (Eq. 11).

2.3 Implementation of the Model in Ansys Fluent

Ansys Fluent is a computational fluid dynamics simulation tool, which can solve various fluid flow and heat transfer tasks. In its native state, it is not prepared to handle our proposed Euler–Euler nanofluid model. However, it does give the user the tools needed to implement such models.

The native Fluent implementation lacks the nanoparticle concentration equation (11). Thus, we first implemented an additional transport equation into Fluent with the User-Defined Scalar Equation for a scalar ϕ. Ansys Fluent solves a transport equation in the following form:

$$\frac{\partial \rho \phi}{\partial t} + \nabla \cdot (\vec{F} \phi - \Gamma_\phi \nabla \phi) = S_\phi, \quad (14)$$

where the terms from the left to right model accumulation, advection, diffusion, and sources. A few modifications of the terms must be made to modify the Ansys version of the transport equation (14) to solve our nanoparticle transport equation (11).

First, we use the DEFINE_UDS_UNSTEADY macro to redefine how the accumulation term is calculated. We define it as follows:

$$\frac{\partial \varphi}{\partial t} = -\int \frac{\partial}{\partial t}(\varphi)dV \approx -\left[\frac{(\varphi)^n - (\varphi)^{(n-1)}}{\Delta t}\right]\cdot \Delta V = -\frac{\Delta V}{\Delta t}\varphi^n + \frac{\Delta V}{\Delta t}\varphi^{n-1}, \quad (15)$$

where $\rho\phi$ in the original implementation (14) is replaced by φ, which in our case represents the volume concentration of the nanoparticles.

With the macro DEFINE_DIFFUSIVITY we can specify the diffusivity Γ_ϕ for the user-defined scalar transport equation. In our case, we model Brownian motion with this term and Γ_ϕ is calculated as

$$\Gamma_\phi = D_B = \frac{k_B T}{3\pi \mu_w d_p}. \quad (16)$$

What remains is the modification of the calculation of the advective term and the inclusion of thermophoretic diffusivity. In Ansys Fluent, we can use the macro DEFINE_UDS_FLUX to define how the advective term is calculated. The macro must specify the advective flux through the face of an element, i.e., the value of $A\vec{F}\cdot n$, where A is the area of the face and $\vec{n}$ is its normal. One can access the advective flux given by the solver using the macro F_FLUX macro: $F_{FL} = A\rho\vec{u}\cdot\vec{n}$. With this, we can define

$$F = \frac{F_{FL}}{\rho} + A\left(\left[0.26\frac{\lambda_w}{(2\lambda_w + \lambda_p)}\frac{\mu_w}{\rho_w}\right]\frac{\nabla T}{T}\right)\cdot\vec{n}. \quad (17)$$

This term represents the transport due to the fluid velocity and an additional transport due to the thermophoretic force. The reason for including the thermophoretic effect in the advective term and not as a source term in the transport equation for the nanoparticle concentration was to ensure that the volume concentration of the nanoparticles is maintained. This formulation was chosen because adding thermophoresis as a source term would falsely imply that particles are generated or lost in the system, which is physically incorrect. Furthermore, a source term can influence the concentration independently of the boundary conditions if a no-flux boundary condition is set for the concentration of nanoparticles on all walls, which leads to unphysical behavior. By including thermophoresis in the advective term, it becomes part of the total particle flux and correctly represents the redistribution of nanoparticles due to the combined effects of bulk fluid motion and thermophoretic drift. This approach maintains the conservation of the volume concentration of the nanoparticles and respects the no-flux boundary conditions. This ensures that particle flow is correctly accounted for without implying its generation or loss, resulting in a model that accurately represents the physical processes involved. Previous studies, such as [22], have not given special attention to the treatment of the thermophoretic term and to the no-flux boundary conditions. They added the thermophoretic term to the Brownian diffusion and prescribed $\partial\varphi/\partial n = -D_T/D_B \partial T/\partial n$.

Using (15), (16), and (17) in (14) enables us to transform the Ansys implementation of a general transport equation to nanoparticle volume fraction transport equation (11).

2.4 Temperature- and Concentration-dependent Fluid Properties of Nanoparticles

The thermophysical nanofluid properties depend on the concentration of the nanoparticles and also on the temperature. Experimental measurements of the thermophysical properties were performed for three different concentrations and for a temperature range between 20 °C and 60 °C and they we extrapolated up to 97 °C. The results are shown in Fig. 6. We used the mixing rule to calculate the density of the nanofluid as follows:

$$\rho_{nf} = \rho_w(1 - \varphi) + \rho_p \varphi, \tag{18}$$

where the density of water depends on temperature (Eq. 9) and the density of solid nanoparticles is constant ($\rho_p = 3970 \, \text{kg} \cdot \text{m}^{-3}$). Based on the experiments performed, we determined predictive expressions for modeling the change in viscosity and thermal conductivity of the nanofluid with the temperature and concentration of the nanoparticles. We found that choosing a second-order polynomial to describe the concentration relationship and a third-order polynomial for the temperature dependence works best. The resulting models are as follows:

$$\left.\begin{array}{l} \mu_{nf} \ [mPa \cdot s] \\ \lambda_{nf} \ [W(mK)] \end{array}\right\} = \left(R_1 \cdot T^3 + R_2 \cdot T^2 + R_3 \cdot T + R_4\right) \times \left(M_1 \cdot \varphi^2 + M_2 \cdot \varphi + M_3\right), \tag{19}$$

with the coefficients R_i and M_i listed in Table 1.

Since the variations of the specific heat capacity with temperature are minimal, a constant value is used for each simulated case. For the case with 0.5% nanoparticle volume concentration, $c_{p,p} = 4119 \, \text{J} \cdot (\text{kg}^{-1}\text{k}^{-1})$ was specified, for 1% 4054 $J \cdot (\text{kg}^{-1}\text{K}^{-1})$ and for 2% 3926 $J \cdot (\text{kg}^{-1}\text{K}^{-1})$. Thermal conductivity of the nanoparticles is $\lambda_p = 25 \, \text{W} \cdot \text{m}^{-1}\text{K}^{-1}$ and their diameter is $d_p = 25 \, nm$.
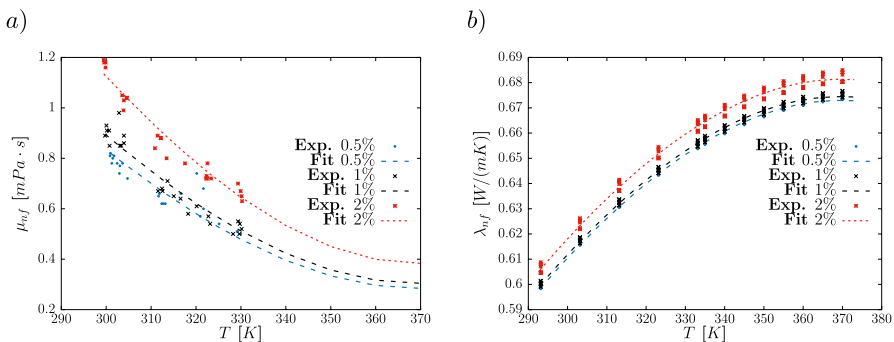
Fig. 6 Measured and extrapolated thermophysical properties of alumina nanofluid: (a) dynamic viscosity and (b) thermal conductivity

Table 1 The coefficients R and M in equation (19) determine the correlation for temperature and concentration dependence of thermal conductivity and viscosity of the nanofluid

Coefficient	λ_{nf} [W $\cdot$ (m^{-1}K^{-1})]	μ_{nf} [mPa $\cdot$ s]
R_1	$-5.443870 \cdot 10^{-3}$	$-5.054417 \cdot 10^{-5}$
R_2	3.015231	$3.759936 \cdot 10^{-2}$
R_3	2.062194	-7.094574
R_4	$9.127901 \cdot 10^{-1}$	$9.644183 \cdot 10^{-1}$
M_1	$1.861615 \cdot 10^{-4}$	-7.092213
M_2	$-6.017123 \cdot 10^{-7}$	$-1.852009 \cdot 10^{-3}$
M_3	$4.882171 \cdot 10^{-6}$	$-7.523715 \cdot 10^{-3}$

2.5 Geometry and Boundary Conditions

From the temperatures measured at the measuring points in the loop, it appears that some of the heat is transferred by conduction through the copper material. For this reason, we have decided that the numerical model has two regions, the fluid region and the copper pipe. The heat is supplied to the lower part of the pipe via an electric resistance heater that is tightly wrapped around the copper pipe. Part of the heat is conducted into the nanofluid and another part travels along the pipe by conduction. The same effect was observed near the pipe section where the cooling jacket is located, where the cooling water absorbs heat from the fluid and the pipe. A sketch of the numerical model can be found in Fig. 4. The loop was made from a copper pipe with an inner diameter of 4.75 *mm* and an outer diameter of 6.36 *mm*. The section where the cooling jacket is located is at the top and is 135 *mm* long. These dimensions were used to create a 3D model of the loop.

The boundary conditions were defined as follows. The outer part of the solid region has the no-flux boundary condition in the isolated section. In the heater section, we specify the power (10, 30, or 50 *W*). For the cooler section, we have used two different boundary conditions. A constant temperature of 21 °C and a convective boundary condition with a heat transfer coefficient of 2000 $\text{W} \cdot (\text{m}^{-2}\text{K}^{-1})$ and an ambient temperature of $21°C$. The inner part of the solid region is in perfect contact with the fluid region, which means that the temperature is continuous across this boundary and that the heat flow is maintained across the boundary. Since the outer boundary of the fluid region is in contact with copper, a no-slip boundary condition was used there. Initially, a uniform distribution of nanoparticles was assumed, so that the volume fraction of nanoparticles was set to 0.5, 1, or 2% everywhere in the fluid region.

3 Model Verification

We devised a one-dimensional test case to verify the implementation of the proposed model into Fluent. Three approaches were compared: The Euler–Euler approach developed in this work, a 1D in-house finite volume method developed in Matlab and a Lagrangian approach, where particle movement is modeled by tracking individual particles.

We consider a stationary nanofluid with constant thermophysical properties in a domain $x \in [0, L]$ heated to a temperature that can be described as

$$T(x) = T_0 + xG, \tag{20}$$

where G is a constant temperature gradient and T_0 the temperature at $x = 0$. If one employs the mixture model (Buongiorno [21]), the equation governing nanoparticle concentration is

$$\frac{\partial \varphi}{\partial t} = \vec{\nabla} \cdot \left(D_B \vec{\nabla}\varphi + D_T \frac{\vec{\nabla}T}{T} \right), \tag{21}$$

where φ is the nanoparticle volume fraction. The Brownian $D_B = aT$ and thermophoretic $D_T = b\varphi$ diffusivities can be estimated using the a and b constants:

$$a = \frac{k_B}{3\pi\mu d_p}, \qquad b = 0.26\frac{k}{2k + k_p}v. \tag{22}$$

Thus, in 1D, we are solving

$$\frac{d\varphi}{dt} = \frac{d}{dx}\left(a(T_0 + xG)\frac{d\varphi}{dx} + \frac{bG}{T_0 + xG}\varphi \right) \tag{23}$$

in a domain $x \in [0, L]$ with no-flux boundary conditions

$$x = 0 : aT_0\frac{d\varphi}{dx} + \frac{bG}{T_0}\varphi = 0, \tag{24}$$

$$x = L : a(T_0 + LG)\frac{d\varphi}{dx} + \frac{bG}{T_0 + LG}\varphi = 0, \tag{25}$$

and an initially constant nanoparticle concentration field

$$\varphi(t = 0) = \varphi_0. \tag{26}$$

For the purpose of this verification experiment, we assume that there is a nanofluid in the domain, with constant thermophysical properties of the same order of magnitude as those of an aluminum oxide nanofluid: $v = 10^{-6}$ m$^{-2} \cdot$ s^{-1}, $\lambda_w = 0.6$ W $\cdot$ m^{-1}k^{-1}, $\lambda_p = 25$ W $\cdot$ mK^{-1}, and d$_p$ = 20nm, which yields $a = 7.38 \cdot 10^{-14}$ m$^2 \cdot$ (s$^{-1} \cdot$ K^{-1}) and b $= 5.95 \cdot 10^{-9} \cdot$ m$^2 \cdot$ s^{-1}. The domain is L = 2.5mm long. The temperature profile inside is linear with $T_0 = 303$ K and G = 16000K $\cdot$ m^{-1}, which relates to a temperature difference of 40 K between the ends of the domain. Starting with $\varphi_0 = 0.03$ we simulate the development of the concentration profile with time governed by equations (23) - (26). We have solved the problem with an in-house 1D implementation of the finite volume method specifically tailored to this problem, by implementing the appropriate conditions in Ansys Fluent, as proposed in this work, and using an in-house Lagrangian particle tracking approach [34]. We compare the concentration profile across the domain for all three methods in Fig. 7 and observe a very good agreement between the results of all three methods, confirming the validity of our novel implementation in Ansys Fluent. The results clearly show that due to thermophoresis the nanoparticle concentration in the direction down temperature gradient is significantly increased.

4 Results

In this section, the numerical results of the simulation of nanofluid flow and heat transfer in the loop are analyzed using different modeling approaches and boundary conditions. The section starts with a grid independence study to ensure the
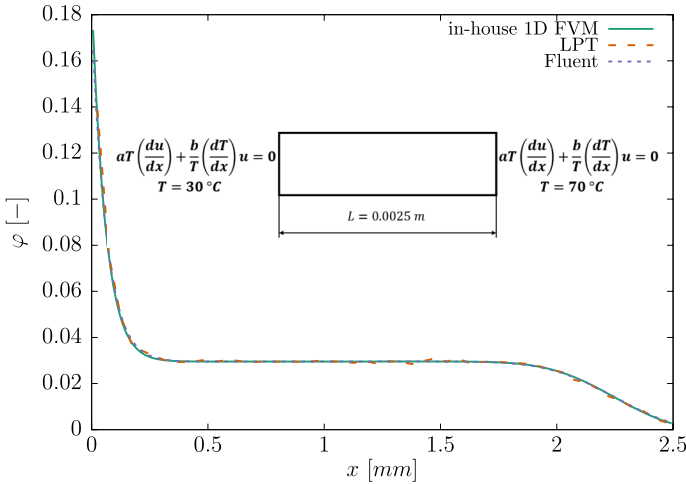
Fig. 7 Nanoparticle concentration profiles in the 1D domain at $t = 1000\ s$. Solutions obtained with an in-house implementation of 1D finite volume method, the Ansys Fluent implementation proposed in this work and a Lagrangian particle tracking (LPT) approach are presented and show good agreement

reliability and accuracy of the computational model. We then analyze the difference between two different boundary condition implementations at the cooling region. Next, we perform a comparative study between the Buongiorno mixture model and the single-phase model using measured thermophysical fluid properties under the boundary condition of a constant temperature to evaluate the differences in the predicted results and assess the impact of additional transport phenomena considered in the Buongiorno model. We then examine the results obtained by applying the Buongiorno mixture model with a convective boundary condition to the cooling region, reflecting more realistic cooling conditions as observed in the experiment. Finally, in the last subsection, a numerical parameter study is presented in which the influence of the nanoparticle diameter d_p on the thermal and fluid properties of the system is investigated.

4.1 Grid Independence Study

To assess numerical accuracy, three structured computational grids with different densities were created, resulting in a final grid with 492800 elements. The coarse grid had 161539 elements, the medium 492800 and the dense 1293120 elements. Figure 8 shows the grid design.

Based on the results obtained, a Richardson extrapolation was performed comparing the maximum temperature of the nanofluid in the system. The element size ratio for the dense and medium grids was 1.38 and 1.45 for the medium and coarse grids, respectively, resulting in a GCI (Grid Convergence Index) of 0.28 % between the fine and medium grids and 0.37 % between the medium and coarse grids. As the differences between all grids considered are almost negligible, a coarse grid

Fig. 8 Presentation of the grid design. Coarse grid has 161 thousand, medium grid has half a million, and fine grid has 1.3 million hexahedral elements
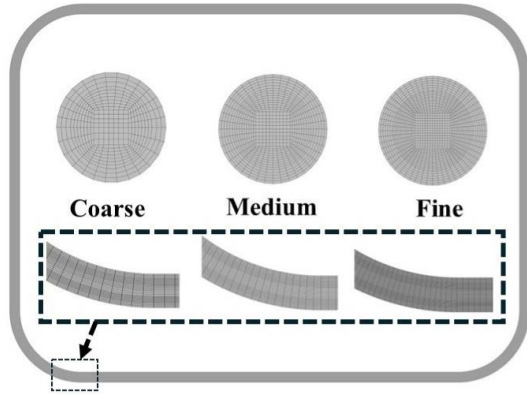

was chosen for the final calculations. The convergence criterion was set to 10^{-6} to ensure the conservation of mass, momentum, energy, and volume concentration of the nanoparticles.

4.2 Constant Temperature Boundary Condition

First we set a Dirichlet type the boundary condition at the cooled region of the loop, choosing a constant value of the temperature there $T = 21$ °C.

4.2.1 The Proposed Mixture Model Results

The predictions of the numerical model for the maximum temperature ($T_5 = T_{max}$) are consistently lower than the experimental measurements, as shown in Fig. 9a. Both the model and the experiments indicate that T_5 increases with the concentration of nanoparticles at lower heat flow rates. At higher heat flow rates, we can observe
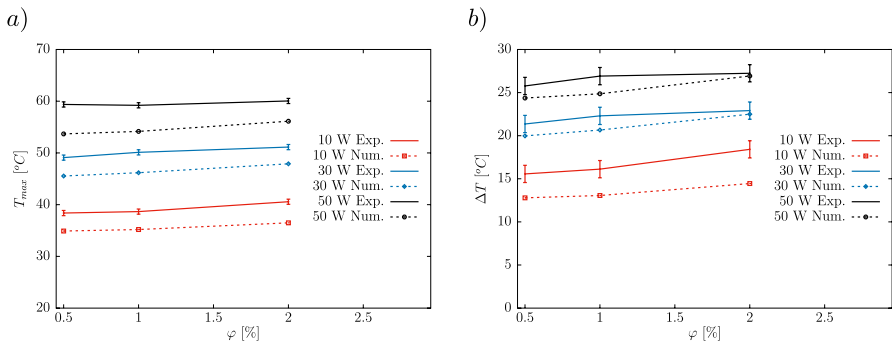
Fig. 9 (a) Temperature in the pipe after the heater T_{max} (b) temperature difference ΔT between the cold leg and hot leg for the case with constant temperature of 21^oC at the cooled section for Buongiorno's mixture model

the same pattern from the numerical results, as the maximum temperature increases with the increase of nanoparticle volume concentration.As for the temperature difference (ΔT) between the cold and hot legs, the model predicts an increase in ΔT at higher nanoparticle volume concentration, as shown in Fig. 9b. The same trend is observed in the experiment. This is due to a decrease in mass flow rate, as shown in Fig. 10b. Since the specific heat is constant for each nanofluid, the decrease in mass flow rate leads to higher temperature differences as the same amount of heat has to be transferred from the heated to the cooled section. As the volume concentration of the nanoparticles increases, the viscosity of the nanofluid increases (see figure 6) leading to higher viscous losses and lower mass flow rates of the nanofluid in the loop. When analyzing the efficiency of the heat exchanger, as shown in Fig. 10b, we find that the efficiency decreases with an increase in heat flow. This behavior is due to the fact that at lower heat flux rates, the length of the cooling section is sufficient for the temperature of the fluid at the end of the cooling section to approach the temperature of the cooling medium. As the heat flow rate increases, less time is available for heat transfer, so the temperature of the fluid downstream of the cooler remains higher, resulting in a lower effectiveness of the heat exchanger. We also find that the effectiveness of the heat exchanger increases with volume concentration of nanoparticles. Nanoparticles increase the thermal conductivity of the fluid and thus improve the heat transfer rate in the heat exchanger. As the concentration of nanoparticles increases, the ability of the fluid to conduct heat improves, allowing for more effective heat exchange between the hot and cold sides. While the higher concentration of nanoparticles can increase the effectiveness of the heat exchanger by promoting better thermal contact and more efficient heat transfer, it must be weighed against the practical limitations of increased flow resistance.

In Fig. 11, we see the temperature distribution inside the loop at three different heating powers (10 *W*, 30 *W*, and 50 *W*). The hot fluid is first heated at the heating section and flows upward along the left leg of the loop. As it rises, the temperature of the fluid increases due to the heat supply. As soon as the fluid reaches the upper end of the loop, it begins to cool down and flows downward along the right-hand leg due to gravity and the cooler environment. This creates a continuous cycle of
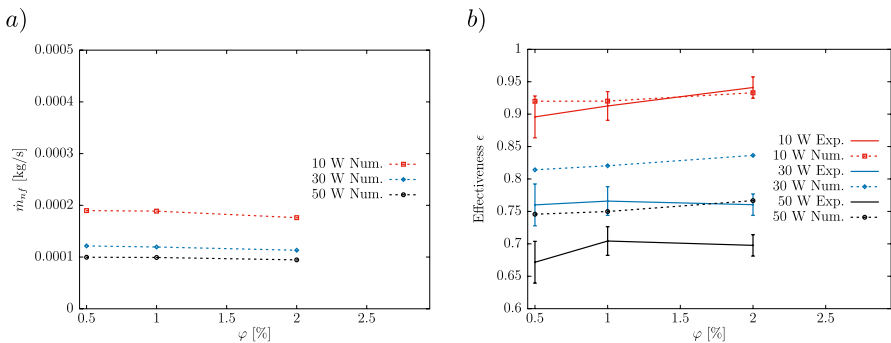

Fig. 10 (a) Mass flow rate of the nanofluid inside the loop $\dot{m}$ and (b) effectiveness ϵ for the case with constant temperature of $21°C$ at the cooled section for Buongiorno's mixture model
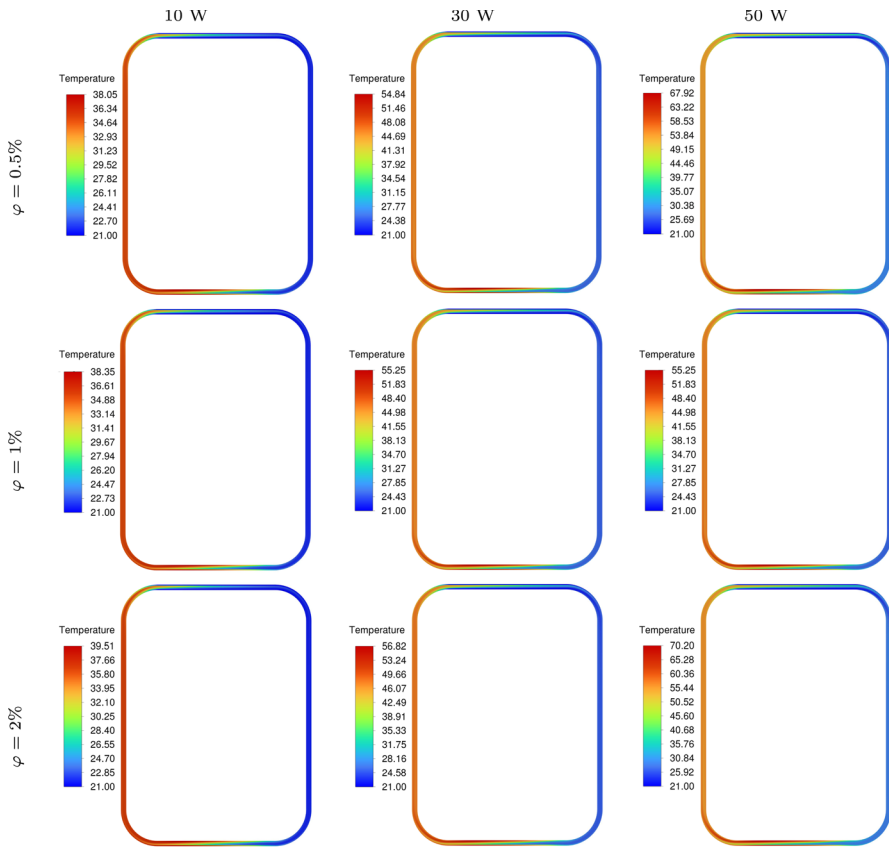
Fig. 11 Comparison of temperature distribution at heating power 10 *W* (left), 30 *W* (center), and 50 *W* (right) with constant temperature boundary condition at the cooler section for three different concentrations: $\varphi = 0.5\%$ (top), $\varphi = 1\%$ (second row), and $\varphi = 0.5\%$ (bottom)

heating, upward flow, cooling, and downward flow within the loop. At a lower heat flow rate of 10 *W*, the temperature gradient within the loop is relatively low. The fluid experiences a gradual increase in temperature as it moves up the left leg and a corresponding decrease along the right leg as it cools. This indicates that the heat transfer at this heat input is moderate. At the highest heat flow rate of 50 *W*, the temperature distribution within the loop becomes even more pronounced. The fluid reaches a higher temperature faster in the heating section and the cooling effect in the cooling section is also more pronounced. This indicates that the heat transfer rate within the loop increases at higher heat flow rates. The strong thermal gradients observed in this heat flow indicate a highly dynamic system in which the heat is transferred and circulates quickly.

Figure 12 shows the distribution of the volume concentration of nanoparticles inside the loop for three different average concentrations of nanoparticles (0.5%, 1%, and 2%) and three different heating powers (10 *W*, 30 *W* and 50 *W*). The analysis
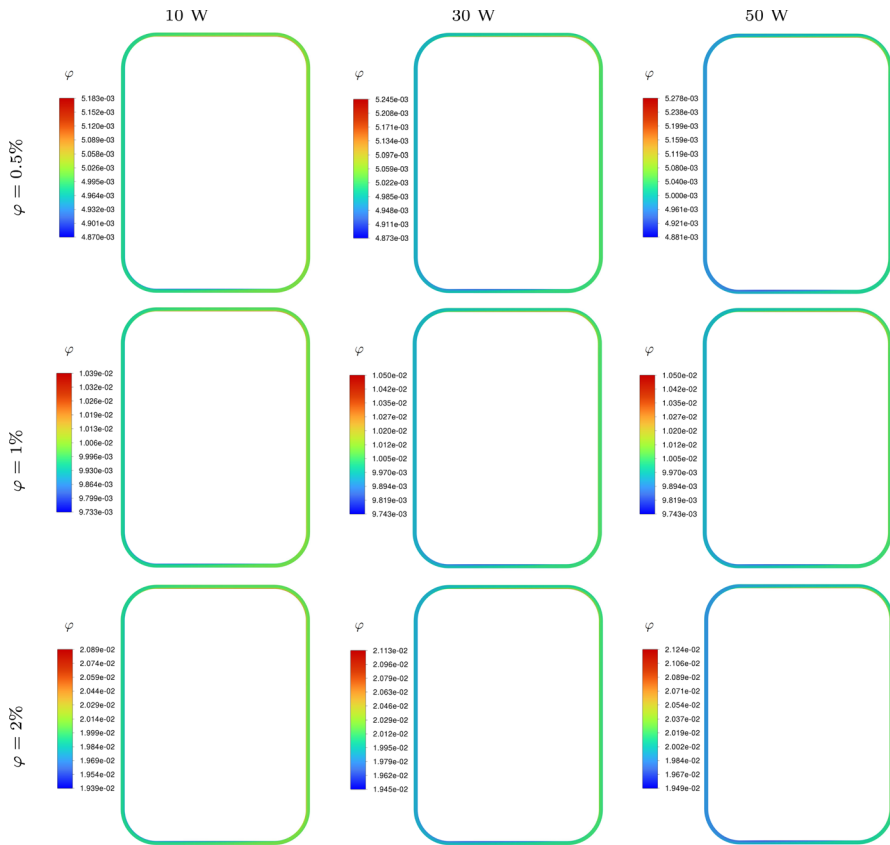
Fig. 12 Comparison of concentration distribution at heat flow rate of 10 *W* (left), 30 *W* (center), and 50 *W* (right) with constant temperature boundary condition at the cooler section for three different concentrations: $\varphi = 0.5\%$ (top), $\varphi = 1\%$ (second row), and $\varphi = 0.5\%$ (bottom)

reveals how the distribution of nanoparticles is affected by different heat flow rates, while the average concentration remains constant in each case. The results show that as the heat flow rate increases, both the maximum and minimum values of the nanoparticle concentration within the loop increase, while the average concentration remains constant at the specified value (e.g., 2% for the case with an average concentration of 2). At the lowest heat flow rate of 10 *W*, the nanoparticle concentration field within the loop remains relatively uniform for each average concentration scenario. The lower heat input creates weaker convective flows, resulting in limited migration or clustering of nanoparticles. In this case, the concentration of nanoparticles is largely determined by diffusion, which maintains a relatively uniform distribution around the average concentration in the loop. The concentration variations are minimal, indicating that the thermal gradients at this low heat input are not sufficient to cause significant transport or accumulation of nanoparticles. As the heat flow rate increases, the variability of the nanoparticle concentration distribution

becomes even more pronounced. The intense convective flows and the stronger thermal gradients lead to a stronger redistribution of nanoparticles due to the combined effects of thermophoresis and Brownian motion. The maximum concentration values reach their highest values at a heat flow of 50 W, indicating an accumulation of nanoparticles in certain regions, while the minimum values continue to decrease, indicating areas where the nanoparticles are less concentrated. Despite these local variations, the average nanoparticle concentration remains constant at the specified value in each case, as expected due to the conservation of mass in the system.

4.2.2 The Single Phase Model Results

The single-phase model assumes that the concentration of nanoparticles is constant over the entire domain. The only change to the CFD simulation is the inclusion of the thermophysical properties of the nanofluid. Although the simplest option, such models have been [35] and still are [36] commonly used among researchers. When comparing Buongiorno's mixture model with the single-phase approach using the measured thermophysical properties of the nanofluid, the results show only negligible differences in several key performance indicators. For the maximum temperatures and the temperature difference ΔT between the cold and hot legs (Fig. 13), both models show very similar predictions, with the results of the Buongiorno model being slightly lower. This indicates that for these parameters, the inclusion of additional transport phenomena such as Brownian motion and thermophoresis in the Buongiorno model does not lead to significant deviations from the simpler single-phase model.

The Buongiorno model also predicts slightly higher values for the mass flow rates compared to the single-phase approach, but the differences are small, as shown in Fig. 14a. This indicates that although the Buongiorno model accounts for more complex interactions between the nanoparticles and the base fluid, these effects have minimal impact on the overall flow properties under the conditions investigated.
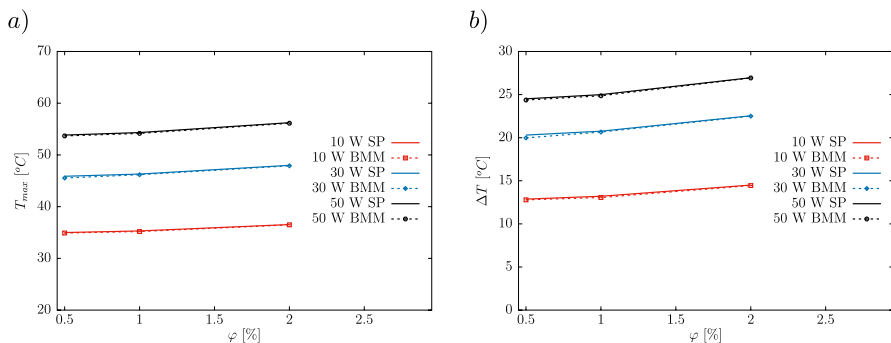
Fig. 13 (a) Temperature in the pipe after the heater T_{max} and (b) temperature difference ΔT between the cold leg and hot leg for the case with constant temperature of $21°C$ at the cooled section for single-phase model compared with results from Buongiorno's mixture model
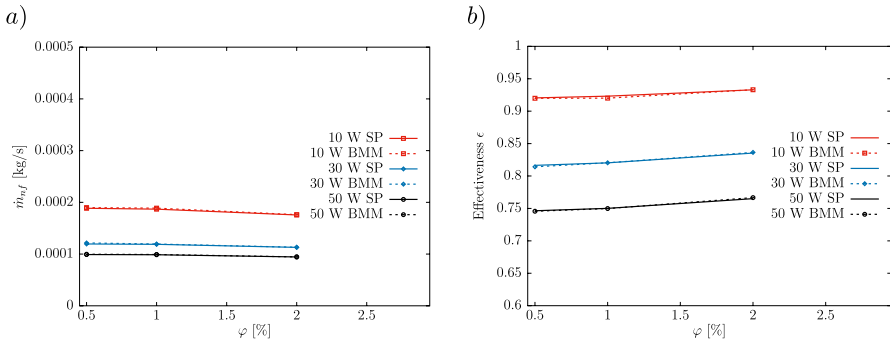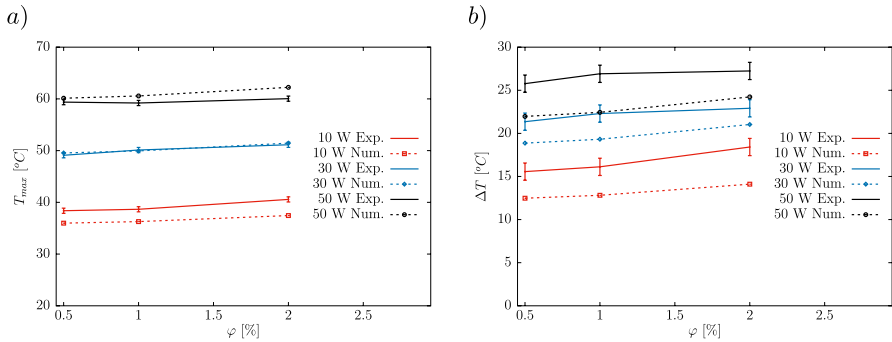
Fig. 14 (a) Mass flow rate of the nanofluid inside the loop $\dot{m}$ (b) effectiveness ϵ for the case with convective boundary condition at the cooled section for Buongiorno's mixture model

With regard to the effectiveness of the heat exchanger (Fig. 14b), the Buongiorno model predicts a slightly lower effectiveness at lower volume concentrations of nanoparticles compared to the single-phase model. However, as the nanoparticle concentration increases, the effectiveness predicted by the Buongiorno model becomes slightly higher. These differences are also negligible, indicating that the additional complexity introduced by the Buongiorno model does not significantly increase the accuracy of the predictions in this context. Overall, the comparison shows that the simpler single-phase approach provides results for the investigated conditions that are very close to those of the more complex Buongiorno mixture model, indicating that the additional computational effort for the latter is not always justified.
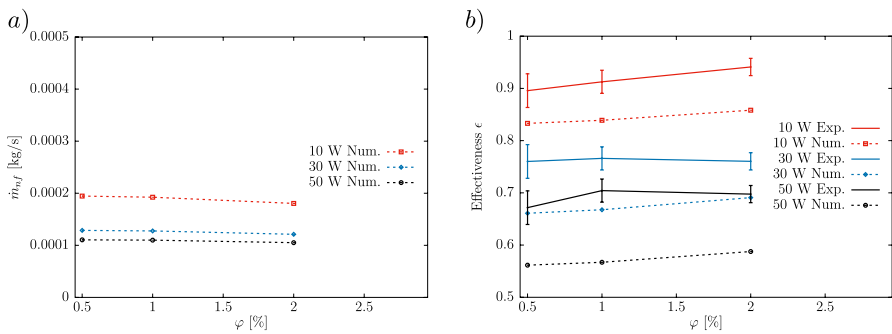
4.3 Convective Boundary Condition at the Cooler

Using Buongiorno's mixture model with a convective boundary condition instead of a constant temperature condition, we have tried to represent more accurately the experimental setup in which cooling takes place via a cooling jacket through which water with a temperature of 21^oC circulates. With a higher heat input, the temperature in the cooling section could rise above 21^oC, so that a constant temperature boundary condition does not necessarily reflect the actual experimental conditions. By applying a convective boundary condition, we have taken into account the dynamic heat transfer between the nanofluid and the cooling medium so that the model can more accurately reflect the variable cooling rates in the experiment. In Fig. 15a, we see that the use of a convective boundary condition brings the maximum temperature predictions closer to the experimentally measured values, indicating that this approach better captures the heat transfer behavior under varying thermal loads. However, in Fig. 15b for the temperature difference (ΔT) between the cold and hot legs, we can see that the differences are higher.

This adjustment also leads to slightly higher predictions for the mass flow rate compared to the constant temperature boundary condition, as observed in Fig. 16a. This could be due to more effective heat removal under the convective condition, as the viscosity of the nanofluid decreases with temperature and thus the mass flow

Fig. 15 (a) Temperature in the pipe after the heater T_{max} and (b) temperature difference ΔT between the cold leg and hot leg for the case with convective boundary condition at the cooled section for Buongiorno's mixture model


Fig. 16 (a) Mass flow rate of the nanofluid inside the loop $\dot{m}$ and (b) effectiveness ϵ for the case with convective boundary condition at the cooled section for Buongiorno's mixture model

rate increases. Despite this slight increase, the difference in mass flow rates remains small, indicating that the convective boundary condition does not drastically change the flow dynamics but improves the thermal predictions.

Regarding the effectiveness of the heat exchanger, we note in Fig. 16b that the differences between the model predictions and the experimental results are more pronounced when using a convective boundary condition.

4.4 Influence of the Particle Size d_p on the Maximum and Minimum Local Concentration

This section deals with the investigation of the influence of particle size on the results. In our case, we analyzed the influence of nanoparticle size on the maximum and minimum local concentration in the system and the maximum temperature in the system. The comparison was performed for the case with constant temperature boundary condition for two different concentrations (0.5 and 2 %) and a heat flow of

a)   b)
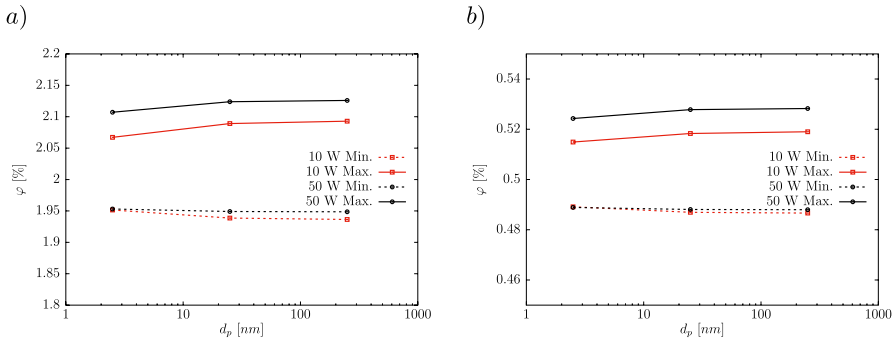
Fig. 17 Maximum and minimum local concentration for heat flow rates of 10 and 50 W and different particle sizes: (a) average nanoparticle concentration of 2% and (b) average nanoparticle concentration of 0.5%

10 W and 50 W. In all cases, the difference between the maximum temperature for each case (different d_p) and the maximum temperature change is negligible, since the maximum temperature in the system changes at the 4 decimal place. However, the particle size affects the maximum and minimum local concentration in the system. In Fig. 17, we see the maximum and minimum local concentrations. As we can see, as the particle size increases, the maximum local concentration in the system increases and the minimum local concentration decreases. The increase and decrease are more pronounced when the particle size increases from 2.5 to 25 nm, the further increase/decrease is less steep when the size is increased to 250 nm. The local maximum concentration increases for all particle sizes considered when the heat flow is increased; the same applies to the local minimum concentration.

5 Conclusion

In this paper, we have presented an implementation of the mixture model for the simulation of flow and heat transfer in a nanofluid. The simulation results were compared with experimental observations of heat transport phenomena in a natural circulation mini loop. Several key findings were obtained.

When modeling the cooling jacket with a constant temperature boundary condition, the mixture model consistently underestimates the maximum temperature (T_5) compared to the experimental data. However, the model effectively captures the temperature trend that increases with the concentration of nanoparticles. This increase in nanoparticle concentration increases the viscosity, decreases the mass flow rate, and increases the temperature difference (ΔT) between the cold and hot legs due to increased flow resistance. The effectiveness of the heat exchanger improves with a higher nanoparticle concentration, as the nanoparticles improve the thermal conductivity. However, increased viscous losses at higher concentrations reduce the overall flow rate and efficiency. The distributions of temperature and nanoparticle concentration show that the distribution remains more uniform at lower heat flow rates. As

the heat flow increases, stronger thermal gradients lead to larger concentration fluctuations due to thermophoresis and Brownian motion.

Comparison of Buongiorno's model with a simpler single-phase model shows minimal differences in the prediction of maximum temperature and mass flow rate. This indicates that the influence of the variable nanoparticle concentration in the fluid due to Brownian motion and thermophoresis is small and the single-phase model might be sufficient for similar nanofluids with low thermal enhancement of the fluid properties.

When a convective boundary condition is applied at the cooling section, the predictions for the maximum temperature become more accurate and better reflect the dynamic heat transfer observed in the experiments. Despite the improved temperature predictions, the changes in the flow dynamics remain minimal.

Finally, the effect of the size of the nanoparticles (d_p) on the local concentration distributions is also noteworthy. While the effect on the maximum temperature of the system is negligible, smaller nanoparticles significantly influence the concentration distributions due to different thermophoretic forces, which are more pronounced at higher heat flow rates.

To summarize, the overall thermal enhancement due to the altered fluid properties for this nanofluid is minimal. Both the Buongiorno mixture model and the single-phase model provide similar predictions for the maximum temperature and flow behavior. Despite the inclusion of Brownian motion and thermophoresis, the Buongiorno model shows only a modest effect on heat transfer, suggesting that a simpler single-phase model may be sufficient to capture the heat transfer dynamics of this system.

Future extensions of this work will focus on broadening the scope of the Euler–Euler model to different types of nanofluids and more complex flow regimes, including turbulent and unsteady conditions. We also plan to extend the model to account for advanced physical phenomena, such as particle aggregation, sedimentation, and electrokinetic effects. We also plan to explore hybrid approaches that combine Euler–Euler and Euler–Lagrange frameworks, which could provide a more detailed representation of nanoparticle–fluid interactions. Finally, the incorporation of machine learning techniques could optimize the prediction of nanofluid behavior, reduce computational effort, and help optimize heat exchanger design.

Data Availability The data generated in this work is available upon request.

Declarations

Conflict of interests The authors declare no conflict of interests.

References

1. S.U.S. Choi, Enhancing thermal conductivity of fluids with nanoparticles. Develop. Appl. Non Newtonian Flows **66**, 99–106 (1995)
2. B.C. Pak, Y.I. Cho, Hydrodynamic and heat transfer study of dispersed fluids with submicron metallic oxide particles. Exp. Heat Transf. **11**, 151–170 (1998)
3. M.H. Buschmann, R. Azizian, T. Kempe, J.E. Juliá, R. Martínez-Cuenca, B. Sundén, Z. Wu, A. Seppälä, T. Ala-Nissila, Correct interpretation of nanofluid convective heat transfer. International Journal of Thermal Sciences 129(June 2017), 504–531 (2018) https://doi.org/10.1016/j.ijthermalsci.2017.11.003
4. E. Abu-Nada, Effects of variable viscosity and thermal conductivity of Al2O3-water nanofluid on heat transfer enhancement in natural convection. Int. J. Heat Fluid Flow **30**, 679–690 (2009). https://doi.org/10.1016/j.ijheatfluidflow.2009.02.003
5. A.T. Utomo, E.B. Haghighi, A.I.T. Zavareh, M. Ghanbarpourgeravi, H. Poth, R. Khodabandeh, B. Palm, A.W. Pacek, The effect of nanoparticles on laminar heat transfer in a horizontal tube. Int. J. Heat Mass Transf. **69**, 77–91 (2014). https://doi.org/10.1016/j.ijheatmasstransfer.2013.10.003
6. M. Awais, A.A. Bhuiyan, S. Salehin, M.M. Ehsan, B. Khan, M.H. Rahman, Synthesis, heat transport mechanisms and thermophysical properties of nanofluids: A critical overview. Int. J. Thermofl. **10**, 100086 (2021). https://doi.org/10.1016/j.ijft.2021.100086
7. M.M. Ali, R. Akhter, M.M. Miah, Hydromagnetic mixed convective flow in a horizontal channel equipped with cu-water nanofluid and alternated baffles. Int. J. Thermofl. **12**, 100118 (2021). https://doi.org/10.1016/j.ijft.2021.100118
8. R. Mulka, G. Beben, B. Zajaczkowski, M.H. Buschmann, Magnetic field influence on heat transfer in inclined laminar ferronanofluid flow. Int. J. Therm. Sci. **205**, 109312 (2024). https://doi.org/10.1016/j.ijthermalsci.2024.109312
9. E. Rajenderan, V.R. Prasad, Numerical study of magneto convective ag (silver) graphene oxide (GO) hybrid nanofluid in a square enclosure with hot and cold slits and internal heat generation/absorption **14**, 24868 https://doi.org/10.1038/s41598-024-76233-z
10. B. Mehta, D. Subhedar, H. Panchal, Z. Said, Synthesis, stability, thermophysical properties and heat transfer applications of nanofluid - A review. J. Mol. Liq. **364**, 120034 (2022). https://doi.org/10.1016/j.molliq.2022.120034
11. A.R.I. Ali, B. Salam, A review on nanofluid: Preparation, stability, thermophysical properties, heat transfer characteristics and application. SN Appl. Sci. **2**, 1636 (2020). https://doi.org/10.1007/s42452-020-03427-1
12. N. Ali, J.A. Teixeira, A. Addali, A Review on Nanofluids: Fabrication, Stability, and Thermophysical Properties. J. Nanomater. **2018**, 1–33 (2018). https://doi.org/10.1155/2018/6978130
13. A.A. Minea, E.I. Cherecheş, A comparative study on thermal behavior of peg 400 and two oxide nanocolloids. Therm. Sci. Engneer. Prog. **55**, 102968 (2024). https://doi.org/10.1016/j.tsep.2024.102968

14. M. Chereches, A. Vardaru, G. Huminic, E.I. Chereches, A.A. Minea, A. Huminic, Thermal conductivity of stabilized PEG 400 based nanofluids: An experimental approach. Int. Commun. Heat Mass Transf. **130**, 105798 (2022). https://doi.org/10.1016/j.icheatmasstransfer.2021.105798

15. S.A. Kadhim, K.A. Hammoodi, A.H. Askar, F.L. Rashid, H.A.A. Wahhab, Feasibility review of using copper oxide nanofluid to improve heat transfer in the double-tube heat exchanger. Results in Engineering, 103227 (2024) https://doi.org/10.1016/j.rineng.2024.103227

16. B. Kamenik, E.B. Elcioglu, A. Turgut, R. Mondragón, L. Hernandez Lopez, J.P. Vallejo, L. Lugo, M.H. Buschmann, J. Ravnik, Numerical analysis of performance uncertainty of heat exchangers operated with nanofluids. Int. J. Thermofl. **14**, 100144 (2022). https://doi.org/10.1016/j.ijft.2022.100144

17. A.A. Minea, B. Buonomo, J. Burggraf, D. Ercole, K.R. Karpaiya, A. Di Pasqua, G. Sekrani, J. Steffens, J. Tibaut, N. Wichmann, P. Farber, A. Huminic, G. Huminic, R. Mahu, O. Manca, C. Oprea, S. Poncet, J. Ravnik, NanoRound: A benchmark study on the numerical approach in nanofluids' simulation. Int. Commun. Heat Mass Transf. **108**, 104292 (2019). https://doi.org/10.1016/j.icheatmasstransfer.2019.104292

18. J. Tibaut, T. Tibaut, J. Ravnik, Numerical simulation of mixed convection of a nanofluid in a circular pipe with different numerical models. J. Therm. Anal. Calorimet. **145**, 2525–2534 (2021). https://doi.org/10.1007/s10973-020-09727-3

19. T.W.B. Riyadi, S.G. Herawan, A. Tirta, Y.J. Ee, A.L. Hananto, P.A. Paristiawan, A.A. Yusuf, H. Venu, I. Veza Irianto, Nanofluid heat transfer and machine learning: Insightful review of machine learning for nanofluid heat transfer enhancement in porous media and heat exchangers as sustainable and renewable energy solutions. Results in Engineering **24**, 103002 (2024). https://doi.org/10.1016/j.rineng.2024.103002

20. S. Nasir, A. Berrouk, A. Aamir, Exploring nanoparticle dynamics in binary chemical reactions within magnetized porous media: A computational analysis **14**, 25505 https://doi.org/10.1038/s41598-024-76757-4 . Accessed 2024-10-29

21. J. Buongiorno, Convective Transport in Nanofluids. J. Heat Transf. **128**, 240–250 (2006)

22. F. Garoosi, L. Jahanshaloo, M.M. Rashidi, A. Badakhsh, M.E. Ali, Numerical simulation of natural convection of the nanofluid in heat exchangers using a Buongiorno model. Appl. Mathemat. Comput. **254**, 183–203 (2015). https://doi.org/10.1016/j.amc.2014.12.116

23. A. Malvandi, D.D. Ganji, Brownian motion and thermophoresis effects on slip flow of alumina/water nanofluid inside a circular microchannel in the presence of a magnetic field. Int. J. Therm. Sci. **84**, 196–206 (2014). https://doi.org/10.1016/j.ijthermalsci.2014.05.013

24. M.A. Sheremet, I. Pop, M.M. Rahman, Three-dimensional natural convection in a porous enclosure filled with a nanofluid using Buongiorno's mathematical model. Int. J. Heat Mass Transf. **82**, 396–405 (2015)

25. F. Mebarek-Oudina, A.S. Preeti Sabu, H. Vaidya, R.W. Lewis, S. Areekara, A. Mathew, A.I. Ismail, Hydromagnetic flow of magnetite-water nanofluid utilizing adapted buongiorno model. Int. J. Modern Phys. B **38**, 2450003 (2024). https://doi.org/10.1142/S0217979224500036

26. D.N. Basu, S. Bhattacharyya, P.K. Das, Development of a unified model for the steady-state operation of single-phase natural circulation loops. Int. J. Heat Mass Transf. **62**, 452–462 (2013). https://doi.org/10.1016/j.ijheatmasstransfer.2013.03.009

27. D.J. Close, The performance of solar water heaters with natural circulation. Solar Energy **6**, 33–40 (1962). https://doi.org/10.1016/0038-092X(62)90096-8

28. N. Izumo, A. Koiwai, Technological background and latest market requirements concerning "static viscosity" measurement with a tuning-fork vibration viscometer. Proceedings of Asia-Pacific Symposium on Measurement of Mass (2009)

29. D.G. Cahill, Thermal conductivity measurement from 30 to 750 K: the 3ω method. Review of Scientific Instruments **61**, 802–808 (1990). https://doi.org/10.1063/1.1141498, https://pubs.aip.org/aip/rsi/article-pdf/61/2/802/19111597/802_1_online.pdf

30. A. Turgut, C. Sauter, M. Chirtoc, J. Henry, S. Tavman, I. Tavman, J. Pelzl, Ac hot wire measurement of thermophysical properties of nanofluids with 3ω method. Europ. Phys. J. Special Topic. **153**, 349–352 (2008). https://doi.org/10.1140/epjst/e2008-00459-7

31. A. Turgut, I. Tavman, M. Chirtoc, H. Karbstein, C. Sauter, S. Tavman, Thermal conductivity and viscosity measurements of water-based tio2 nanofluids. Int. J. Thermophys. **30**, 1213–1226 (2009). https://doi.org/10.1007/s10765-009-0594-2

32. O. Engineering, The Temperature Handbook vol. 29. Stamford, CT: Omega Engineering Inc, ??? (1995)

33. N. şobanoğlu, Z.H. Karadeniz, Effect of nanofluid thermophysical properties on the performance prediction of single-phase natural circulation loops. Energies **13**(10) (2020) https://doi.org/10.3390/en13102523

34. J. Wedel, P. Steinmann, M. Štrakl, M. Hriberšek, J. Ravnik, Shape matters: Lagrangian tracking of complex nonspherical microparticles in superellipsoidal approximation. International Journal of Multiphase Flow 158(September 2022), 104283 (2023) https://doi.org/10.1016/j.ijmultiphaseflow.2022.104283

35. J. Ravnik, L. Škerget, M. Hriberšek, Analysis of three-dimensional natural convection of nanofluids by bem. Engineer. Anal. Bound. Elem. **34**(12), 1018–1030 (2010). https://doi.org/10.1016/j.enganabound.2010.06.019

36. N. Talem, S. MIHOUB, L. Boumia, A. Safa, J. Navas, P. Estellé, Z. Benayad, Thermal performance of parabolic trough collector using oil-based metal nanofluids. Appl. Therm. Engineer. **256**, 124128 (2024). https://doi.org/10.1016/j.applthermaleng.2024.124128

Authors and Affiliations

Blaž Kamenik[1] · Nejc Vovk[1] · Elif Begum Elcioglu[2] · Firat Sezgin[2] · Erdem Ozyurt[2] · Ziya Haktan Karadeniz[3] · Alpaslan Turgut[4] · Jure Ravnik[1]

✉ Jure Ravnik
  jure.ravnik@um.si

  Blaž Kamenik
  blaz.kamenik@um.si

  Nejc Vovk
  nejc.vovk@um.si

  Elif Begum Elcioglu
  ebelcioglu@eskisehir.edu.tr

  Firat Sezgin
  fsezgin@eskisehir.edu.tr

  Erdem Ozyurt
  eozyurt@eskisehir.edu.tr

  Ziya Haktan Karadeniz
  haktankaradeniz@iyte.edu.tr

  Alpaslan Turgut
  alpaslan.turgut@deu.edu.tr

[1] Faculty of Mechanical Engineering, University of Maribor, Maribor, Slovenia

[2] Department of Mechanical Engineering, Eskişehir Technical University, Eskişehir, Turkey

[3] Department of Energy Systems Engineering, Izmir Institute of Technology, Izmir, Turkey

[4] Department of Mechanical Engineering, Dokuz Eylul University, Izmir, Turkey